Journal of MATERIALS RESEARCH

Invited Feature Paper
DOI:10.1557/s43578-025-01725-1

EARLY CAREER SCHOLARS IN MATERIALS SCIENCE

ANNUAL ISSUE

# PEG surface functionalization of $Bi_2S_3$ nanorods: Structural characterization, cytocompatibility, and radiosensitizing potential

Isabel Galain[1,2], Camila Pérez Saint Esteven[1], Natalia Sanchez Moreno[2], Wilner Martínez López[3], Valtencir Zucolotto[2], María Eugenia Pérez Barthaburu[4], Ivana Aguiar[1,a)]

[1] Área Radioquímica, Facultad de Química, Universidad de La República, Montevideo, Uruguay
[2] Grupo de Nanomedicina e Nanotoxicologia, Instituto de Física de São Carlos, Universidade de São Paulo, São Carlos, Brazil
[3] Genetics Department and Biodosimetry Service, Instituto de Investigaciones Biológicas Clemente Estable, Montevideo, Uruguay
[4] Departamento de Desarrollo Tecnológico, Centro Universitario Regional del Este, Universidad de La República, Rocha, Uruguay
[a)] Address all correspondence to this author. e-mail: iaguiar@fq.edu.uy

Received: 3 July 2025; accepted: 9 October 2025; published online: 3 November 2025

**Bismuth sulfide nanorods are promising for biomedical use due to their high atomic number and biocompatibility. This paper presents their surface modification through ligand exchange with polyethylene glycol (PEG) of various molecular weights to enhance dispersibility and biocompatibility in physiological media. PEGylation was confirmed, ensuring structural integrity. The optimized formulation maintained morphology, with a hydrodynamic size of 134 nm and a zeta potential of –11.3 mV. Stability and interaction in DMEM with fetal bovine serum and artificial plasma were evaluated, showing a reversible protein corona with low association constants. Cytotoxicity assays showed minimal toxicity across concentrations. The radiosensitizing effect of PEGylated nanorods was tested under three X-ray doses, revealing a dose-dependent increase in cancer cell death, with dose enhancement factors of 1.3 and 1.6 for MCF7 and A549 cells respectively, at a survival factor of 37. These findings support PEGylated $Bi_2S_3$ nanorods as stable, biocompatible platforms for enhancing radiotherapy efficacy.**

Ivana Aguiar

Ivana Aguiar is an Associate Professor at Radiochemistry Area, Facultad de Química, Universidad de la República, Uruguay, since 2021. She has been working at this institution since 2005. She received her degree in Chemistry in 2006, her M.Sc. in Chemistry in 2008, and her Ph.D. in Chemistry in 2013, all from Facultad de Química, Universidad de la República, where she was appointed Assistant Professor in 2007. With a strong commitment to fostering a sustainable world, she specializes in the synthesis of nanoparticles and the study of their interactions with different forms of radiation. Ivana has been thoroughly involved with the Materials Science and Technology community through volunteer work in Materials Research Society. She has built a strong network of collaborations to advance interdisciplinary research in Uruguay, focusing on the development of ionizing radiation detectors, nanostructured photocatalysts, and radiosensitizers aimed at improving the efficiency of radiotherapy. She has also been instrumental in organizing the first two Materials Science Researchers Meetings in Uruguay, in 2018 and 2023. Alongside her teaching responsibilities in materials science and nanotechnology, she actively engages in outreach activities to connect with the wider community, in activities as "What is nano? and the National Crystal Growing Competition, in which she has participated since 2014.

## Introduction

Cancer remains the second leading cause of death worldwide, with nearly 10 million deaths reported in 2020 according to the World Health Organization. Radiotherapy is a widely used therapeutic modality, employed in over half of all cancer treatments [1]. However, its effectiveness is frequently constrained by the need to limit radiation exposure to surrounding healthy tissues, which restricts the maximum therapeutic dose deliverable to tumors. This challenge has motivated the development of different strategies, including the radiosensitizing agents [2]. These agents can enhance the local effects of ionizing radiation selectively within tumor tissues [3].

Among these strategies, nanomaterials containing high atomic number (Z) elements have shown significant promise as radiosensitizers. Their potential lies in their ability to amplify radiation-induced damage through enhanced photoelectric absorption, secondary electron emission, and reactive oxygen species (ROS) generation [4]. Bismuth sulfide ($Bi_2S_3$) in particular, stands out for this purpose, due to bismuth's high atomic number (Z = 83), excellent X-ray attenuation capacity, intrinsic chemical stability, and favorable biocompatibility profile. $Bi_2S_3$ nanostructures have demonstrated radiosensitizing effects in *in vivo* and preclinical models by increasing localized radiation dose and promoting ROS-mediated cytotoxicity in cancer cells [5, 6].

While several synthetic routes have been developed for the preparation of $Bi_2S_3$ nanostructures—including hydrothermal, solvothermal, and hot-injection approaches—translation of these materials to biomedical applications requires more than structural control [7, 8]. Surface properties play a critical role in determining biological interactions, including biodistribution, cellular uptake, and immune recognition. A key factor influencing nanoparticle circulation time is the formation of the protein corona—a dynamic layer of biomolecules that adsorbs onto the nanoparticle surface upon exposure to biological fluids. This corona modifies physicochemical properties such as size and surface charge, effectively redefining the nanoparticle's biological identity and dictating its interaction with cells and biological barriers [9]. The presence of opsonins can promote clearance by phagocytic cells, whereas selective enrichment of specific plasma proteins may reduce immune recognition. While PEGylation is commonly used to extend circulation time by reducing protein adsorption, it does not entirely prevent corona formation, and its effectiveness depends on factors such as PEG molecular weight and surface density [10, 11].

To modulate protein corona composition and improve *in vivo* performance, surface functionalization with biocompatible ligands has proven essential. Polyethylene glycol (PEG), a hydrophilic polymer widely used in nanomedicine, can reduce nonspecific protein adsorption, enhance colloidal stability in physiological environments, and prolong systemic circulation by evading immune clearance [12, 13].

In this work, we investigate the functionalization of $Bi_2S_3$ nanorods with polyethylene glycol (PEG) with different molecular weights. We provide a comprehensive structural and surface characterization of $Bi_2S_3$ PEG functionalized nanorods and evaluate their behavior in complex biological media, with particular attention to protein corona formation and surface charge modulation. Finally, we assess the cytotoxicity of the PEGylated nanorods in healthy and cancerous human cell lines and examine their radiosensitizing effect under different X-ray irradiation doses. Our findings contribute to the rational design of surface-engineered nanomaterials for advanced biomedical applications, particularly in the new advanced radiotherapy treatments.

## Results and discussion

### Nanorod characterization and ligand exchange

Ligand exchange with PEG, using either low (400 g/mol) or high (4000 g/mol) molecular weight variants, was verified by FTIR spectroscopy (Fig 1) for all the samples. The presence of characteristic C–O–C and C–C–O vibrational bands confirmed successful PEGylation. At 1101 $cm^{-1}$ and 611 $cm^{-1}$ we observed the PEG 400 C–O–C stretching and bending bands respectively. The same bands but for PEG 4000 were observed at 1111 and 617 $cm^{-1}$. Regarding the C–C–O bands, we observed them at 1034 and 525 $cm^{-1}$ for PEG 400 and at 1061 and 530 $cm^{-1}$ for PEG 4000 [14, 15]. Complete ligand exchange was achieved for PEG 400 after 4 h and for PEG 4000 after 24 h of reaction. Intermediate spectra at 4 h with PEG 4000 showed similarities with the $Bi_2S_3$-$PEG_{400}$, suggesting partial exchange and a time-dependent reorganization of PEG on the nanoparticle surface. However, these particles exhibited significant handling challenges; their isolation was particularly difficult, and substantial material losses were observed during purification. Consequently, we opted to proceed with further characterization and biological studies using $Bi_2S_3$ nanoparticles coated with $PEG_{4000}$, which demonstrated greater stability and recoverability.

Thermal analysis by DSC-TG of samples with PEG 4000 and different reflux time provided further evidence of surface modification, as can be seen in Fig. 1 (c and d). An increase in the organic content from 14 to 32% was observed for PEG 4000-functionalized nanorods when the reaction time increased from 4 to 24 h, indicating a higher degree of PEG coating. This trend is supported by small endothermic peaks in the DSC curves. Additionally, in both 4 and 24 h samples, a mass loss of approximately 5–6% was detected at lower temperatures, which may be attributed to residual OLA that was not completely exchanged. This interpretation is further supported by small endothermic events observed around 300 °C in the DSC

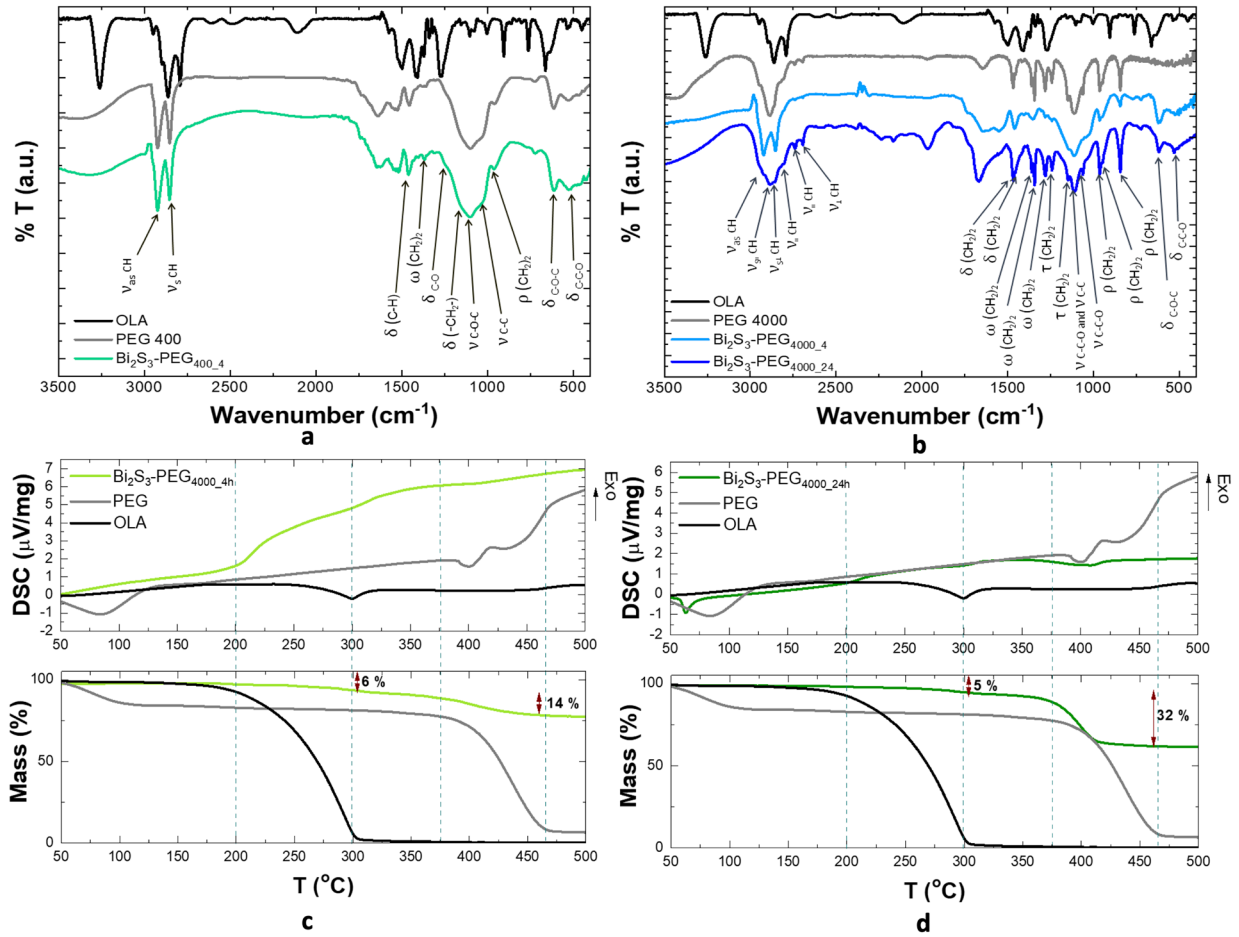


**Figure 1:** (a) FTIR spectra of nanoparticles with PEG 400 and (b) with PEG 4000, prepared at different reflux time, in comparison with the spectra of the corresponding PEG and OLA, (c) DSC-TG for sample with reflux time 4 h, (d) DSC-TG for sampe with reflux time 24 h.

curves. This OLA signal is not observable in the IR spectra, possibly due to its low concentration and overlap with the dominant PEG absorption bands. Despite that, these results verified effective surface functionalization and improved dispersibility, which is essential for ensuring suspension stability and biocompatibility in biological environments. Taking all this into account, and knowing that the PEG improves dispersibility and biocompatibility, all subsequent analyses were conducted using the $Bi_2S_3$-$PEG_{4000\_24}$ sample.

TEM analysis of sample $Bi_2S_3$-$PEG_{4000\_24}$ showed uniform nanorods with well-defined morphology and narrow size distribution; an image of the nanorods can be seen in Fig. 2. The size distribution was fitted to lognormal, with an average size of 3.6 and a standard deviation 0.6 nm. We confirmed that the rod morphology after the ligand exchange has been maintained.

The crystalline identity of the $Bi_2S_3$-$PEG_{4000\_24}$ nanorods was confirmed by XRD and Raman spectroscopy [Fig 3(a and b), respectively]. In the XRD diagram, we can see that the positions of the peaks agree with the ones of the ICSD file 89,324. Besides, a characteristic broadening of the peaks is observed, which correlates with the nanometric size of the particles [16]. The vibrational modes observed in Raman spectra summarized in Table S1 are consistent with reported $Bi_2S_3$ lattice vibrations [17, 18]. Results of hydrodynamic size and Z potential are presented in Table 1 and in Fig. S1 of Supplementary Information. In all cases, a correlation between the results obtained by DLS and NTA was observed, despite the differences between the techniques. DLS measurements tend to yield slightly larger sizes due to their intensity-weighted nature, which emphasizes larger particles, whereas NTA provides number-based distributions that more accurately reflect the actual particle population, particularly in polydisperse systems. Furthermore, the sample $Bi_2S_3$-$PEG_{4000\_24}$ exhibited a slightly negative Z-potential of − 11,3 (± 5,82) mV, which is advantageous for potential intravenous administration of the radiosensitizer, as neutral or negatively charged nanoparticles exhibit enhanced stability due to reduced plasma protein adsorption (i.e., reduced opsonization) and lower nonspecific cellular uptake, which together contribute to prolonged circulation times [19, 20].

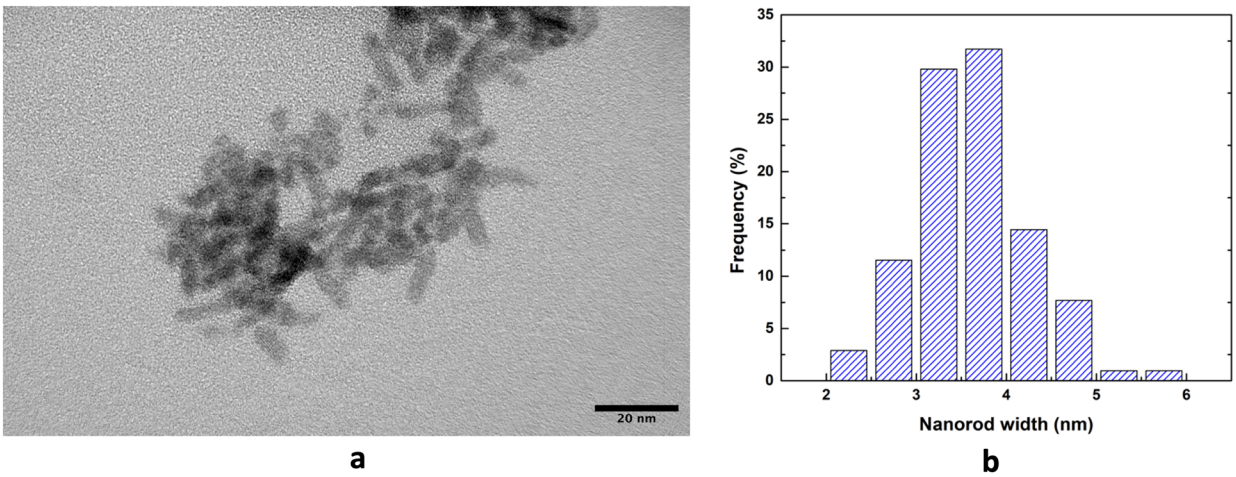


**Figure 2:** (a) TEM image of $Bi_2S_3$-$PEG_{4000\_24}$ nanorods and (b) particle size distribution histogram.

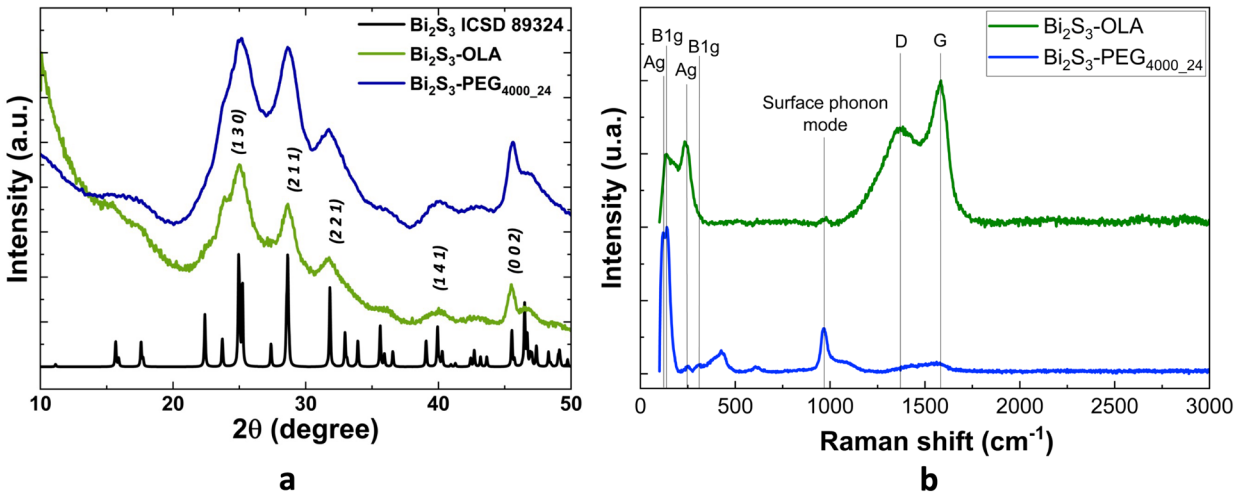


**Figure 3:** (a) XRD diagram with the main peaks indexed and (b): Raman spectra of sample $Bi_2S_3$-$PEG_{4000\_24}$ with PEG4000 and OLA as ligands.

**TABLE 1:** Zeta potential and particle size obtained by DLS and NTA of PEG-4000 and OLA-coated nanoparticles.

| Nanoparticle | Z (mV) | Size by DLS (nm) | Size by NTA (nm) |
|---|---|---|---|
| $Bi_2S_3$-OLA | − 3,62 (± 0,56) | 278,0 (± 78,8) | 133,8 (± 56,2) |
| $Bi_2S_3$-$PEG_{4000\_24}$ | − 11,3 (± 5,82) | 124,4 (± 28,1) | 134,1 (± 64,2) |

## Protein corona formation

To evaluate nanoparticle interaction with biological media, sample $Bi_2S_3$-$PEG_{4000\_24}$ was incubated in DMEM with 10% FBS and in artificial blood plasma (aBPF). DLS and zeta potential measurements were taken over 48 h (Fig4 and Table 2). The hydrodynamic size remained stable in both media, with values ranging between 122–242 nm, and zeta potential values between –26.5 and –6.1 mV, indicating good behavior of the suspension in the solvents and moderate surface charge.

The absence of significant aggregation and minimal shifts in surface charge imply limited nonspecific protein adsorption, consistent with the formation of a soft corona.

ITC is a label-free, in-solution technique that quantitatively measures the heat change associated with molecular interactions under constant temperature. When applied to the study of protein adsorption onto nanoparticles, ITC enables the direct characterization of the thermodynamics of corona formation, including the binding affinity ($K_a$), binding enthalpy variation (ΔH) and entropy (ΔS). This data provides insights into the driving forces governing protein-nanoparticle interactions, which are crucial for understanding nanoparticle behavior in biological environments and their biocompatibility. In this work, ITC (Table 3 and Figure S2) revealed exothermic interactions

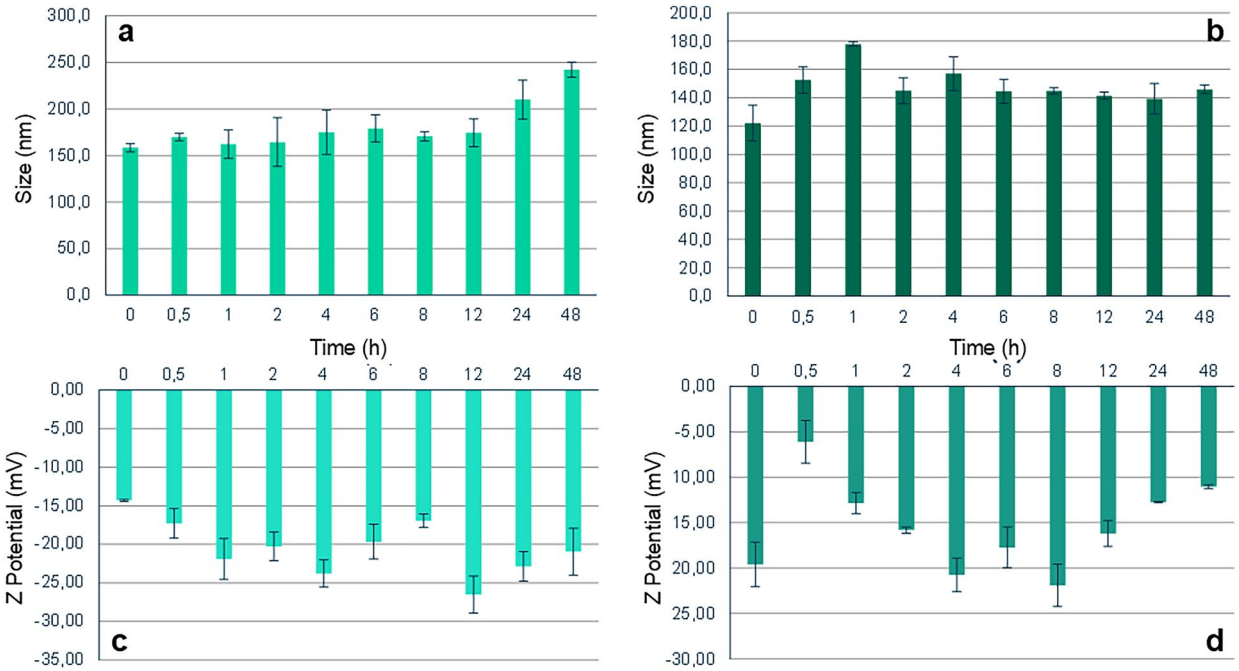


**Figure 4:** DLS and zeta potential of $Bi_2S_3$-$PEG_{4000\_24}$ nanorods in (a, b) DMEM + FBS and (c, d) artificial blood plasma.

**TABLE 2:** DLS and zeta potential of $Bi_2S_3$ nanorods in biological media.

| Nanoparticle | Medium | Size range (nm) | Zeta potential range (mV) |
|---|---|---|---|
| $Bi_2S_3$-$PEG_{4000\_24}$ | DMEM + FBS | 158.4—242.2 | − 26.5 to − 14.3 |
| $Bi_2S_3$-$PEG_{4000\_24}$ | aBPF | 122.2—177.9 | − 21.9 to − 6.1 |

**TABLE 3:** Binding Enthalpy (ΔH), entropy (ΔS), and association constant (K) data for the interaction of $Bi_2S_3$-PEG with DMEM medium containing 10% FBS and aBPF.

| Nanoparticles | Medium | ΔH (kcal/mol) | ΔS (cal/mol°C) | $K_a$ ($kM^{-1}$) |
|---|---|---|---|---|
| $Bi_2S_3$-$PEG_{4000\_24}$ | DMEM + SFB | − 34.1 | − 95.7 | 12.1 |
| $Bi_2S_3$-$PEG_{4000\_24}$ | aBPF | − 2121 | − 7100 | 0.72 |

($\Delta H < 0$) and unfavorable entropy changes ($\Delta S < 0$) for both media, which means that the interactions between the fluids and the nanoparticles are enthalpically favoured. It also confirms that Van der Waals forces, electrostatics, and hydrogen bonding are the main drivers of corona formation [21, 22]. As it was expected, the association constant for aBPF is lower than the one for DMEM + FBS, indicating that the association is stronger for the media with proteins. However, the low value of association constants for both media ($K_a = 12.1\ kM^{-1}$ in DMEM + FBS and $0.72\ kM^{-1}$ in aBPF) confirm the absence of strong binding or extensive desolvation effects. These results are consistent with a reversible and weakly adsorbed soft corona, largely mediated by the PEG surface layer. They also align with other findings where a reduced number of proteins and a less complex protein pattern were found on PEGylated PLGA nanoparticles [9].

This weak corona is advantageous in systemic applications, as it minimizes immune recognition, reduces opsonization, and promotes prolonged circulation. Overall, the data demonstrate that PEGylation provides effective steric stabilization of $Bi_2S_3$ nanorods and supports their use as a platform for biomedical applications requiring controlled nano–bio interactions.

## Cytotoxicity assays

Firstly, we determined the nanoparticles uptake by confocal microscopy. Images of the MCF7 and A549 cells showing the $Bi_2S_3$-$PEG_{4000\_24}$ nanoparticles inside the cells (representative concentration of 25 and 50 μg/mL) are showed in Fig. S3. The biocompatibility of PEGylated $Bi_2S_3$ nanorods was assessed using two cancer cell lines (MCF7 and A549) and three non-cancerous cell lines (MRC5, BHK-570, and HepaRG), as is shown in Fig. 5. In normal cell lines, PEG-coated $Bi_2S_3$ nanoparticles exhibited generally low cytotoxicity, though some variability was observed depending on the cell type. BHK-570 cells showed a clearer dose- and time-dependent decrease in viability, while MRC5 cells displayed only modest effects at higher concentrations and longer exposures. HepaRG cells were the most tolerant, with viability largely maintained across conditions except for slight reductions at the highest doses. The nanoparticles also exhibited time- and dose-dependent

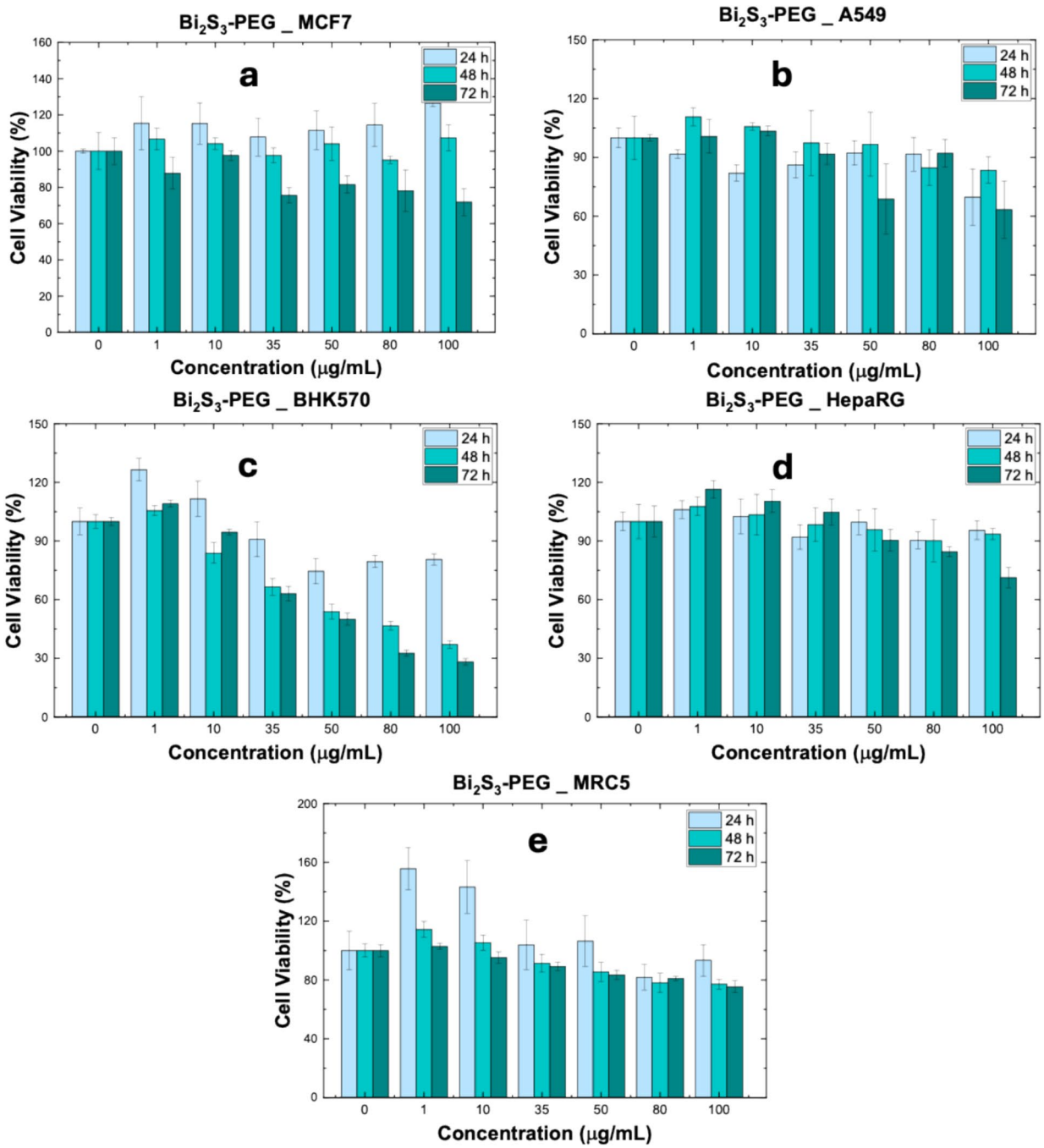


**Figure 5:** Cell viability of MCF-7, A549, BHK-570, HepaRG and MRC5 cells after 24, 48 and 72 h of exposure to $Bi_2S_3$-$PEG_{4000\_24}$ nanorods. Differences were considered statistically significant at $p < 0.05$.

effects on cell viability in both MCF7 and A549 cancer cell lines. While MCF7 cells showed minimal response at early time points, a slight decrease in viability was observed at later time points. In contrast, A549 cells were more responsive, showing subtle changes in viability over time and a progressive trend throughout the experiment. A more detailed explanation of the statistical treatment is explained in tables S2 and S3. Given the size of the nanorods, their primary elimination route is expected to be hepatic rather than renal, making this observation unlikely to pose a limitation for future *in vivo* applications. These results support the low intrinsic cytotoxicity of $Bi_2S_3$ and demonstrate that PEG surface functionalization does not introduce additional toxicity. The inclusion

of multiple healthy cell lines further reinforces the biosafety profile of the material and supports its potential for selective radiosensitization in therapeutic contexts.

## Radiosensitization studies

To evaluate the radiosensitizing potential of PEGylated $Bi_2S_3$ nanorods, MCF7 and A549 cells were irradiated with X-rays at doses of 0, 2, 4, and 8 Gy, 24 h after nanoparticle exposure. The MTT assay showed a dose-dependent reduction in viability in nanoparticle-treated groups compared to irradiated-only ones [Fig 6 (a and b)] for A549 cells. In MCF7 cells, no strong dependence of cell death on radiation dose was observed at 48 h after irradiation; however, a dose-dependent variation became apparent 72 h post-irradiation.

Despite the inherent difficulty of comparing radiosensitizing efficacy across studies due to differences in experimental design, cell lines, radiation sources, and nanoparticle concentrations, the NER values obtained for our PEGylated $Bi_2S_3$ nanorods indicate promising performance. At a concentration of nanoparticles of 100 μg/mL and with an irradiation dose of 2 Gy, NER values of 1.42 (MCF7) and 1.21 (A549) were recorded at 48 h post-irradiation, increasing to 1.95 and 1.39 respectively at 72 h. Compared to our previous work using $Bi_2S_3$-PVP nanorods (NER = 1.71 at 2 Gy), the PEGylated system offers a similar radiosensitizing effect, considering that this results were obtained using a different evaluation method (MTT assay), as opposed to the Trypan Blue assay used in our previously reported work, but with the added advantages of improved dispersibility [5]. Still, our current values compare favorably with previous reports, such as $Bi_2S_3$@$SiO_2$ mesoporous nanoparticles (NER = 1.36–1.48 with 50 μg/mL and P-32 irradiation for 24–72 h) and $Bi_2S_3$@BSA-FA-CUR (NER = 1.14–1.67 under 2–6 Gy with 50 μg/mL) [23, p. 3], [24, p. 3]. Notably, higher NERs reported for $Bi_2S_3$-PLGA (up to 7.64) required significantly higher nanoparticle concentrations (up to 5 mg/mL) [25]. Altogether, these findings underscore the potential of PEGylated $Bi_2S_3$ nanorods as effective and biocompatible radiosensitizers.

These findings demonstrate that PEG-coated $Bi_2S_3$ nanorods can act as effective radiosensitizers *in vitro*, enhancing the cytotoxic effects of ionizing radiation in cancer cells without harming healthy cells at therapeutic concentrations. These results

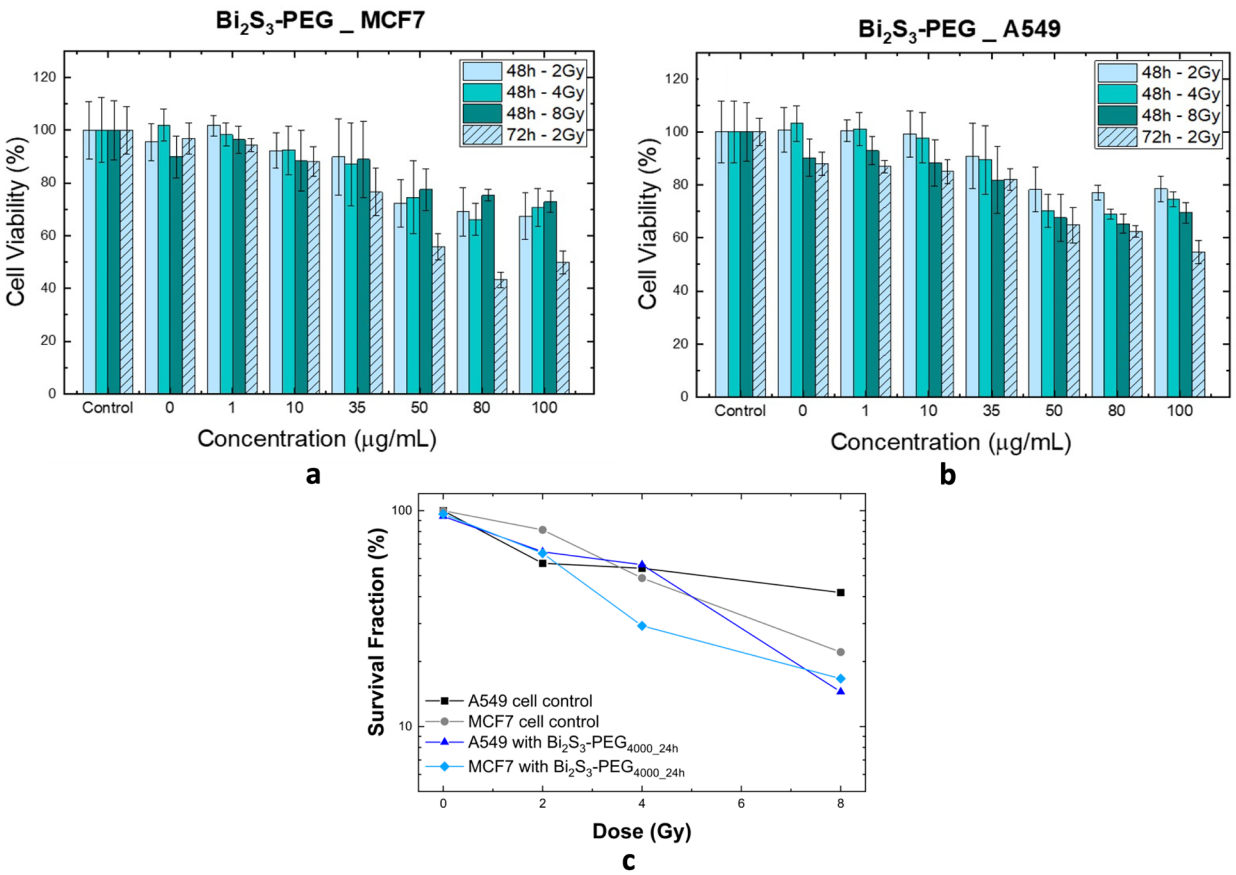


**Figure 6:** (a) Cell viability of MCF7 and (b) A549 cell lines obtained by the MTT assay, irradiated in the presence of nanorods $Bi_2S_3$-$PEG_{4000\_24}$ with 2, 4 or 8 Gy, evaluated after 48 and 72 h after irradiation (differences were considered statistically significant at $p < 0.05$); (c) survival curves as a function of radiation dose for A549 and MCF7 cell lines treated with $Bi_2S_3$-$PEG_{4000\_24}$ nanorods, obtained from clonogenic assay.

support their continued development for advanced radiotherapy treatments.

The clonogenic survival curves [see Fig6 (c)] clearly demonstrate that pre-treatment with $Bi_2S_3$-$PEG_{4000\_24}$ nanorods significantly enhances the radiosensitivity of both A549 and MCF7 cancer cells. In the absence of nanorods (control), both cell lines exhibited a dose-dependent reduction in survival fraction, but retained a relatively high proliferative capacity, especially at intermediate radiation doses (2–4 Gy). However, when cells were pre-treated for 24 h with $Bi_2S_3$-$PEG_{4000\_24}$ nanorods, a marked decrease in survival was observed across all radiation doses, indicating effective radiosensitization.

The radiosensitizing effect was more pronounced in the MCF7 breast cancer cells, which showed a sharper drop in survival fraction, particularly at 4 Gy and 8 Gy, suggesting a higher susceptibility of this cell type to the synergistic action of radiation and $Bi_2S_3$-$PEG_{4000\_24}$ nanorods. In contrast, A549 lung cancer cells exhibited a more moderate, yet consistent, radiosensitizing response. These differences may reflect intrinsic variations in DNA repair efficiency, redox status, or nanorods uptake between the two cell lines.

The $Bi_2S_3$-PEG formulation used in this study showed effective performance without causing significant toxicity in the absence of radiation (as suggested by the similar survival at 0 Gy between treated and control groups in the clonogenic assay), reinforcing its potential as a biocompatible radiosensitizer. Taken together, these findings support the utility of $Bi_2S_3$-PEG nanorods as a promising platform for enhancing radiotherapy efficacy, especially in tumors that are typically resistant to conventional radiation doses.

The calculated Dose Enhancement Factors (DEF) provide quantitative evidence of the radiosensitizing effect induced by $Bi_2S_3$-$PEG_{4000\_24}$ nanoparticles in both A549 and MCF7 cell lines. In MCF7 breast cancer cells, a DEF of 1.3 was observed at both $SF_{37}$ (surviving fraction at 37%, a standard reference point in radiobiology, that corresponds to the radiation dose at which the fraction of surviving cells decreases to 37% of the initial population, assuming an exponential survival curve) and $SF_{50}$ (surviving fraction at 50%), indicating a consistent enhancement in radiosensitivity across moderate and higher survival thresholds. This suggests that the PEGylated $Bi_2S_3$ nanorods sensitize MCF7 cells to radiation in a dose-independent manner within this range. In contrast, A549 lung cancer cells exhibited a DEF of 1.6 at $SF_{37}$ and 1.2 at $SF_{50}$, reflecting a more pronounced radiosensitizing effect at lower survival fractions. This differential suggests that the nanoparticles are particularly effective in reducing clonogenic capacity at higher radiation doses in A549 cells. The higher DEF observed in A549 cells at $SF_{37}$, compared to MCF7, highlights cell-line-specific responses to $Bi_2S_3$-$PEG_{4000\_24}$ nanoparticles and supports their potential utility in enhancing the therapeutic ratio of radiotherapy. Overall, the DEF values obtained fall within a biologically relevant range, supporting the use of PEGylated bismuth sulfide nanorods as promising radiosensitizers for both breast and lung cancer models.

A well-established mechanism for inorganic nanoparticles acting as radiosensitizers involves the production of secondary emissions due to their high-Z nature and interaction with radiation. In the case of PEGylated $Bi_2S_3$ nanoparticles, cell death can be induced either through the direct disruption of DNA by the ionizing radiation itself or by these secondary emissions, or via the generation of reactive oxygen species (ROS) upon interaction with the biological environment. Significant ROS generation has been observed for bismuth sulfide nanoparticles in combination with radiotherapy [26, 27], supporting their potential role as radiosensitizers. A schematic overview of the proposed mechanism is presented in Fig. S4.

This work highlights several key aspects relevant to the development of functional nanomaterials. First, the choice of synthetic method directly impacts the crystallinity, aspect ratio, and surface chemistry of the resulting nanostructures. The hot-injection approach used here enables precise control over nucleation and growth kinetics, resulting in uniform nanorods with high crystallinity, which is essential for consistent optical and electronic behavior.

Moreover, surface engineering through ligand exchange represents a critical strategy for tuning interfacial interactions between nanoparticles and their surrounding environment. The ability to switch from hydrophobic (OLA) to hydrophilic ligands (PEG) allows tailoring of behavior without compromising structural integrity. The PEG coating, in particular, not only improves stability but also enhances biocompatibility and stealth behavior, reducing protein adsorption and immune clearance—features directly translatable to drug delivery and imaging applications.

This study exemplifies how systematic characterization—combining TEM, DLS, FTIR, and zeta potential analysis—can be used to establish clear structure–function relationships. Understanding how nanoscale morphology and surface chemistry influence macroscopic behavior (e.g., stability, cytotoxicity, protein corona formation) is central for advancing in the rational design of nanomaterials for targeted biomedical applications.

PEGylation remains one of the most established strategies to improve the stability and pharmacokinetics of nanomedicines, and several PEGylated drugs are already approved and used in clinical practice [28]. Nevertheless, growing evidence indicates that PEG can induce anti-PEG antibodies, potentially accelerating clearance or triggering hypersensitivity reactions. Similar responses have also been reported for several proposed PEG alternatives, suggesting that immunogenicity is not an issue exclusive to PEG. Importantly, the clinical impact of these reactions is highly context-dependent, influenced by formulation type, dose, administration route, and patient immune status. In this regard, PEGylated $Bi_2S_3$ nanoparticles show translational

potential due to their improved colloidal stability, reduced opsonization, and prolonged circulation, which may favor tumor accumulation, while the very low solubility of the $Bi_2S_3$ core may limit acute ion-related toxicity. At the same time, the long-term fate of these nanoparticles *in vivo* is not yet fully established, as PEG coatings may undergo gradual desorption or oxidative degradation, altering nanoparticle–protein interactions, and although extensive dissolution of $Bi_2S_3$ is unlikely, partial surface transformation or limited ion release cannot be excluded. Together, these considerations indicate that PEG-coated $Bi_2S_3$ nanoparticles are promising candidates for biomedical applications, while also highlighting the importance of complementary *in vivo* studies to clarify their clearance pathways, immunogenicity, and long-term biosafety.

## Conclusions

This study presents a systematic approach for developing stable and biocompatible suspensions of $Bi_2S_3$ nanorods, aiming at their applications as radiosensitizers in biomedical settings. Using a hot-injection synthesis, we produced uniform nanorods and functionalized their surfaces via ligand exchange with PEG. Comprehensive characterization by TG/DSC and FTIR confirmed successful functionalization, while DLS analysis demonstrated the stability of the nanoparticle suspension.

Among the tested formulations, $Bi_2S_3$-$PEG_{4000\_24}$ emerged as the most suitable candidate for biological evaluation due to its recoverability, enhanced functionalization, superior stability, minimal aggregation, and compatibility with physiological environments. Collectively, these findings highlight the potential of PEG-modified $Bi_2S_3$ nanorods for biomedical applications requiring prolonged circulation time, reduced immune recognition, and predictable nano–bio interactions.

*In vitro* assays confirmed high cell viability across a wide range of concentrations, and protein corona studies showed negligible changes in particle size and surface charge over 48 h. The $Bi_2S_3$-$PEG_{4000\_24}$ nanorods significantly increase the radiosensitivity of cancer cells without inducing notable toxicity in the absence of radiation. The effect was observed in both lung and breast cancer cell lines, with a stronger response in the latter, suggesting cell-type-specific differences in susceptibility. These findings establish a robust formulation and processing strategy for $Bi_2S_3$ nanorods, supporting their future application in preclinical *in vivo* studies for enhanced radiotherapy.

Overall, the systematic evaluation of surface chemistry, solvent environment, and processing conditions demonstrates the importance of integrating physicochemical parameters when designing nanomaterials for biomedical use. This integrative characterization approach bridges the gap between nanoscale structure and macroscopic biological function, advancing the rational design of nanomaterials for theranostic applications.

## Materials and methods

### Synthesis of $Bi_2S_3$ nanorods

$Bi_2S_3$ nanorods were synthesized via a hot-injection method previously reported [5]. Briefly, the bismuth precursor solution was prepared by dissolving Bismuth neodecanoate (10 mM, Aldrich, 99%) in 20 mL of octadecene (ODE, Aldrich, 90%) and 5 mL of oleic acid (OA, Aldrich, 90%). This mixture was heated to 180 °C under a Nitrogen atmosphere. The sulfur precursor, consisting of elemental sulfur powder (50 mM, Aldrich) dissolved in 2.5 mL of oleylamine (OLA, Aldrich, > 98%) and 10 mL of ODE, was rapidly injected into the hot bismuth solution. The reaction proceeded for 40 s before being quenched with 70 mL of cold toluene and rapidly cooled with compressed air. Nanorods were recovered by centrifugation and washed multiple times with a mixture of ethanol (EtOH) and ethyl acetate (EtOAc) prior to characterization.

### Ligand exchange

Ligand exchange from OLA to polyethylene glycol (PEG), either Mw ~ 400 or Mw ~ 40,000, Aldrich was performed. Nanorods were dispersed in 90 mL of a 2:1 EtOH:EtOAc mixture containing 17.5 mM of the selected ligand and refluxed at 130 °C for 4 or 24 h, according to Table 4. The suspension was cooled, centrifuged, and washed repeatedly with EtOH:EtOAc.

### Characterization

X-ray diffraction (XRD) analysis was conducted using a PANalytical Empyrean diffractometer with Cu Kα radiation (λ = 1.5418 Å) in Bragg–Brentano geometry over a 2θ range of 10°–50°. The identity of the samples was also confirmed by Raman spectroscopy (inVia Raman confocal microscope, Renishaw). Morphology and size were evaluated via transmission electron microscopy (TEM) and high-resolution TEM (HRTEM) using a JEOL 2100 microscope operated at 200 kV. The hydrodynamic size and Z potential of nanoparticles was determined by dynamic light scattering (DLS, Zetasizer Nano-SZ90 from Malvern Panalytical) and nanoparticle tracking analysis (NTA, NS300 Nanosight). Samples were drop-casted onto carbon-coated copper grids. ImageJ (v1.51w) was used for image analysis. The presence of the ligands, both before and after the ligand exchange procedure was analyzed by diffuse infrared

**TABLE 4:** Ligand exchange conditions.

| Sample | Molecular weight (g/mol) | Time (h) |
|---|---|---|
| $Bi_2S_3$-$PEG_{400}$ | 400 | 4 |
| $Bi_2S_3$-$PEG_{4000\_4}$ | 4000 | 4 |
| $Bi_2S_3$-$PEG_{4000\_24}$ | 4000 | 24 |

spectroscopy (Shimadzu IRPrestige-21, with a diffuse reflectance DiffusIR Pike Technology accessory). Thermogravimetry (TG) and differential scanning calorimetry (DSC) analyses were used to quantify and study ligands' thermal decomposition events. A Netzsch F5 TGDSC simultaneous thermal analyzer was used, with 7.4 mg of sample in an alumina pan, under 50 mL/ min of nitrogen flow rate, and heated from room temperature up to 400 °C.

### Protein corona formation

Protein corona formation was studied by measuring DLS and zeta potential (Zetasizer Nano-SZ90 from Malvern Panalytical) after dispersing nanoparticles in DMEM with 10% FBS or in aBPF, which has a ionic concentration similar to blood [29]. These studies were carried out with a nanoparticle concentration of 50 μg/mL and an incubation time between 0 and 48 h, by triplicate. Isothermal titration calorimetry experiments (ITC, Microcalorimeter ITC200, Malvern Instruments Ltd) were performed to investigate the interactions between $Bi_2S_3$-PEG nanoparticles with DMEM medium containing 10% FBS and aBPF.

### Cell culture

Human cancer cell lines MCF-7 (mammary adenocarcinoma, ATCC® HTB-22™) and A549 (lung carcinoma, ATCC® CCL-185™), and normal cell lines Hepa-RG (human liver fibroblasts, ATCC® HB-8065™) and BHK-570 (hamster kidney fibroblasts, ATCC® CRL-10314™) and MRC5 (human lung fibroblasts, ATCC® CCL-171™) were cultured in Dulbecco's Modified Eagle Medium (DMEM, PanReac AppliChem) with Phenol red as pH indicator and supplemented with 10% fetal bovine serum (FBS), 100 U/mL penicillin, and 100 μg/mL streptomycin.

### Microscope confocal images

MCF7 and A549 cells were seeded on sterile coverslips in 24-well plates ($1 \times 10^4$ cells/well) and incubated overnight. Cells were incubated during 24 h with $Bi_2S_3$-$PEG_{4000\_24}$ nanoparticles at 25 and 50 μg/mL for 24 h at 37 °C/5% $CO_2$. After that, cells were fixed with 4% paraformaldehyde during 10 min and washed twice with PBS. The membrane was stained with CellMask Deep Red Plasma Membrane Stain ($\lambda_{ex}/\lambda_{em} = 649/666$ nm, Thermo Fischer Scientific) and nuclei with Hoechst 33,342 ($\lambda_{ex}/\lambda_{em} = 350/461$ nm, Thermo Fischer Scientific). Images were acquired using a confocal fluorescence microscope (Zeiss LSM 710) with 40 × oil-immersion objectives, in bright field and excitation lasers at 405 nm and 633 nm. Image analysis was carried out with Zen 3.2 Blue edition Software.

### Cytotoxicity assay

Cells were seeded into 96-well plates at a density of $2.5 \times 10^4$ cells/mL and incubated in a humidified atmosphere at 37 °C with 5% $CO_2$. After 24 h, nanorods suspensions were added. Following incubation, medium was removed, and cells were incubated with 0.5 mg/ml MTT reagent for two hours. Formazane crystals were dissolved in dimethyl sulfoxide and the sample absorbance was measured at 540 nm.

Cytotoxicity was evaluated by MTT assay after 24, 48 and 72 h incubation with $Bi_2S_3$ nanorods at six concentrations ranging from 1 to 1000 μg/mL. A control group without nanoparticles was included. All assays were carried out in triplicate and repeated independently three times. Results were expressed as the mean values and SD deviation.

### Radiosensitization studies

MCF7 and A549 cells were incubated as previously mentioned. Cells were incubated 24 h after seeded, with nanoparticles $Bi_2S_3$-PEG4000_24, and after another 24 h cells were irradiated with a small animal irradiator (Precision, X-Rad225XL) with doses of 2, 4 or 8 Gy. Cells viability was evaluated by MTT assay 48 and 72 h after irradiation. All assays were carried out in triplicate and repeated independently three times. Results were expressed as the mean values and SD deviation. The nanoparticle-mediated enhanced ratio (NER) was calculated as the cell viability after radiotherapy/the viability after radiotherapy + nanoparticles.

### Statistical analyses

All statistical analyses were performed using the RStudio software (RStudio version 2024.12.0 + 467). Data were analyzed using one-way ANOVA to determine significant differences among groups. Post hoc comparisons were conducted using Tukey's honestly significant difference (HSD) test to identify pairwise differences between means. Grouping of means was performed using compact letter display (CLD) to represent statistically significant differences between treatments, using the agricolae package. The Interaction effect was analyses using a generalized lineal model (GLM). Results were considered statistically significant at $p < 0.05$.

### Clonogenic assay

A clonogenic assay was performed to evaluate the long-term proliferative capacity of A549 and MCF7 cells after exposure to $Bi_2S_3$-$PEG_{4000\_24}$ nanoparticles (50 μg/mL) and ionizing radiation (0, 2, 4, and 8 Gy). 300 cells/well were seeded in a 6 well plate, incubated overnight, treated with nanoparticles for

24 h, and then irradiated. The cells were incubated until colonies formed (10 days for A549 and 14 days for MCF7), with the medium replaced every two days. Colonies were fixed with 4% of paraformaldehyde (PFA, Aldrich), washed with PBS, and stained using a hematological kit (Laborclin). For MCF7 and A549 cells, two independent replicates were performed and the results were expressed as the mean values. Stained wells were scanned and analyzed using ImageJ (v1.53c) with a custom macro: ROI = 1100 px, contrast enhancement = 1%, background subtraction = 10 px, noise = 2 px, Renyi Entropy threshold (cut-off = 197), and particle analysis with circularity 0.3–1.0. Plating efficiency (PE) and surviving fraction (SF) were calculated using standard formulas. SF values were fitted and the dose enhancement factor (DEF) were calculated as the dose to produce an effect without nanoparticles/Dose to produce the same effect with nanoparticles.

## Acknowledgments

Authors thank to Comisión Sectorial de Investigación (CSIC) from Universidad de la República, Programa de Desarrollo de las Ciencias Básicas (Pedeciba), Agencia Nacional de Investigación (ANII) and Comisión Académica de Posgrado (CAP) for funding. We also thank to Heinkel Bentos Pereira from CURE for XRD measurements, Dr. Mauricio Rodríguez from CURE for DSC-TG measurements, Alvaro Olivera from High Resolution Microscopy Laboratory for TEM images, MSc. Raphael Guimarães Lopes from CEPOF-IFSC, USP, for samples irradiation.

## Author contributions

I. Galain, I. Aguiar and M. E. Pérez Barthaburu contributed to the conceptualization and design of the study. I. Galain and C. Pérez Saint Esteven carried out the synthesis and functionalization of nanorods and the *in vitro* biological assays. I. Galain and N. Sánchez Moreno conducted the physicochemical assays. W. Martínez López collaborated with the biological assays. Data analysis was carried out by I. Galain and C. Pérez Sain Esteven. I. Galain, C. Pérez Sain Esteven, V. Zucolotto, M. E. Pérez Barthaburu and I. Aguiar participated in the discussion of the results. The manuscript was written by I. Aguiar and revised critically by all authors. All authors read and approved the final version of the manuscript.

## Funding

Comisión Sectorial de Investigación Científica (CSIC), Universidad de la República, Project 24520250100048UD, Comisión Académica de Posgrado (CAP), PhD Scholarship, Agencia Nacional de Investigación e Innovación, Mobility Scholarships MOV_CA_2022_1_175212 and MOV_CA_2020_1_163032.

## Data availability

All relevant data generated and analyzed during this study are included in this article and its supplementary information and is available on request.

## Declarations

**Conflict of interest** On behalf of all authors, the corresponding author states that there is no conflict of interest.

## Open Access



## Supplementary Information

The online version contains supplementary material available at https://doi.org/10.1557/s43578-025-01725-1.

## References

1. "WHO report on cancer: setting priorities, investing wisely and providing care for all", World Health Organization, 2020.
2. S.M.S. Mousavi-Kiasary et al., Synergistic cancer therapies enhanced by nanoparticles: advancing nanomedicine through multimodal strategies. Pharmaceutics **17**(6), 682 (2025). https://doi.org/10.3390/pharmaceutics17060682
3. H. Zhang et al., A systematic review on the development of radiosensitizers, with cancer selectivity, for radiotherapy using ionizing radiation. AIMS Bioeng. **10**(2), 89–110 (2023). https://doi.org/10.3934/bioeng.2023008
4. M. He et al., Advances in nanoparticle-based radiotherapy for cancer treatment. iScience **28**(1), 111602 (2025). https://doi.org/10.1016/j.isci.2024.111602
5. I. Galain et al., Enhancement of radiation response of breast cancer cells through the incorporation of $Bi_2S_3$ nanorods. J. Nanopart. Res. **24**(3), 68 (2022). https://doi.org/10.1007/s11051-022-05455-x

6. Y. He et al., 3-bromopyruvate-loaded bismuth sulfide nanospheres improve cancer treatment by synergizing radiotherapy with modulation of tumor metabolism. J. Nanobiotechnol. **21**(1), 209 (2023). https://doi.org/10.1186/s12951-023-01970-8
7. M. Sahu, C. Park, A comprehensive review on bismuth-sulfide-based compounds. Mater. Today Sustain. **23**, 100441 (2023). https://doi.org/10.1016/j.mtsust.2023.100441
8. M.-A. Shahbazi et al., The versatile biomedical applications of bismuth-based nanoparticles and composites: therapeutic, diagnostic, biosensing, and regenerative properties. Chem. Soc. Rev. **49**(4), 1253–1321 (2020). https://doi.org/10.1039/C9CS00283A
9. K. Partikel et al., Effect of nanoparticle size and PEGylation on the protein corona of PLGA nanoparticles. Eur. J. Pharm. Biopharm. **141**, 70–80 (2019). https://doi.org/10.1016/j.ejpb.2019.05.006
10. T. Kopac, Protein corona, understanding the nanoparticle–protein interactions and future perspectives: a critical review. Int. J. Biol. Macromol. **169**, 290–301 (2021). https://doi.org/10.1016/j.ijbiomac.2020.12.108
11. R.K. Mishra, A. Ahmad, A. Vyawahare, P. Alam, T.H. Khan, R. Khan, Biological effects of formation of protein corona onto nanoparticles. Int. J. Biol. Macromol. **175**, 1–18 (2021). https://doi.org/10.1016/j.ijbiomac.2021.01.152
12. J. Hu, S. Liu, Emerging trends of discrete poly(ethylene glycol) in biomedical applications. Curr. Opin. Biomed. Eng. **24**, 100419 (2022). https://doi.org/10.1016/j.cobme.2022.100419
13. B. Rezaei et al., Effect of polymer and cell membrane coatings on theranostic applications of nanoparticles: a review. Adv. Healthc. Mater. (2024). https://doi.org/10.1002/adhm.202401213
14. W.H.T. Davison, Infrared spectra and crystallinity Part III. Poly(ethylene glycol). J. Chem. Soc. Resumed (1955). https://doi.org/10.1039/jr9550003270
15. T. Miyazawa, K. Fukushima, Y. Ideguchi, Molecular vibrations and structure of high polymers. III. Polarized infrared spectra, normal vibrations, and helical conformation of polyethylene glycol. J. Chem. Phys. **37**(12), 2764–2776 (1962). https://doi.org/10.1063/1.1733103
16. S.V. Koniakhin, O.I. Utesov, I.N. Terterov, A.V. Siklitskaya, A.G. Yashenkin, D. Solnyshkov, Raman spectra of crystalline nanoparticles: replacement for the phonon confinement model. J. Phys. Chem. C **122**(33), 19219–19229 (2018). https://doi.org/10.1021/acs.jpcc.8b05415
17. B. Xu, G. Wang, H. Fu, 23327Enhanced photoelectric conversion efficiency of dye-sensitized solar cells by the incorporation of flower-like Bi2S3:Eu3+ sub-microspheres. Sci. Rep. **6**(1), 23395 (2016). https://doi.org/10.1038/srep23395
18. I. Zumeta-Dubé, J.-L. Ortiz-Quiñonez, D. Díaz, C. Trallero-Giner, V.-F. Ruiz-Ruiz, "First order Raman scattering in bulk $Bi_2S_3$ and quantum dots: reconsidering controversial interpretations." J. Phys. Chem. C **118**(51), 30244–30252 (2014). https://doi.org/10.1021/jp509636n
19. R.R. Arvizo et al., "Modulating pharmacokinetics, tumor uptake and biodistribution by engineered nanoparticles." PLoS ONE **6**(9), e24374 (2011). https://doi.org/10.1371/journal.pone.0024374
20. M.A. Dobrovolskaia, S.E. McNeil, Immunological properties of engineered nanomaterials. Nat. Nanotechnol. **2**(8), 469–478 (2007). https://doi.org/10.1038/nnano.2007.223
21. D. Prozeller, S. Morsbach, K. Landfester, Isothermal titration calorimetry as a complementary method for investigating nanoparticle–protein interactions. Nanoscale **11**(41), 19265–19273 (2019). https://doi.org/10.1039/C9NR05790K
22. A. Velázquez-Campoy, H. Ohtaka, A. Nezami, S. Muzammil, E. Freire, Isothermal titration calorimetry. Curr. Protoc. Cell Biol. (2004). https://doi.org/10.1002/0471143030.cb1708s23
23. M. Ma et al., $Bi_2S_3$ -embedded mesoporous silica nanoparticles for efficient drug delivery and interstitial radiotherapy sensitization. Biomaterials **37**, 447–455 (2015). https://doi.org/10.1016/j.biomaterials.2014.10.001
24. H. Nosrati, J. Charmi, M. Salehiabar, F. Abhari, H. Danafar, Tumor targeted albumin coated bismuth sulfide nanoparticles ($Bi_2S_3$) as radiosensitizers and carriers of curcumin for enhanced chemoradiation therapy. ACS Biomater. Sci. Eng. **5**(9), 4416–4424 (2019). https://doi.org/10.1021/acsbiomaterials.9b00489
25. M. Yao et al., Multifunctional $Bi_2S_3$/PLGA nanocapsule for combined HIFU/radiation therapy. Biomaterials **35**(28), 8197–8205 (2014). https://doi.org/10.1016/j.biomaterials.2014.06.010
26. K. Wang, A.T. Jalil, M.M. Saleh et al., Glutathione (GSH) conjugated $Bi_2S_3$ NPs as a promising radiosensitizer against glioblastoma cancer cells". Chem. Pap. **77**, 1921–1928 (2023). https://doi.org/10.1007/s11696-022-02592-4
27. F. Gao, D. Wang, T. Zhang et al., F"acile synthesis of Bi2S3-MoS2 heterogeneous nanoagent as dual functional radiosensitizer for triple negative breast cancer theranostics". Chem. Eng. J. **395**, 125032 (2020)
28. D. Shi, D. Beasock, A. Fessler, J. Szebeni, J.Y. Ljubimova, K.A. Afonin, M.A. Dobrovolskaia, To PEGylate or not to PEGylate: immunological properties of nanomedicine's most popular component, polyethylene glycol and its alternatives. Adv. Drug Deliv. Rev. **180**, 114079 (2022). https://doi.org/10.1016/j.addr.2021.114079
29. A. Oyane, H.-M. Kim, T. Furuya, T. Kokubo, T. Miyazaki, T. Nakamura, Preparation and assessment of revised simulated body fluids. J. Biomed. Mater. Res. **65A**, 188–195 (2003). https://doi.org/10.1002/jbm.a.10482